

# Evaluating Sparse Autoencoders for Monosemantic Representation

**Moghis Fereidouni<sup>1</sup>, Muhammad Umair Haider<sup>1</sup>, Peizhong Ju<sup>1</sup>, A.B. Siddique<sup>1</sup>**

<sup>1</sup>University of Kentucky

moghis.fereidouni@uky.edu, muhammadumairhaider@uky.edu, peizhong.ju@uky.edu, siddique@cs.uky.edu

## Abstract

A key barrier to interpreting large language models is polysemanticity, where neurons activate for multiple unrelated concepts. Sparse autoencoders (SAEs) have been proposed to mitigate this issue by transforming dense activations into sparse, more interpretable features. While prior work suggests that SAEs promote monosemanticity, there has been no quantitative comparison with their base models. This paper provides the first systematic evaluation of SAEs against base models concerning monosemanticity. We introduce a fine-grained concept separability score based on the Jensen–Shannon distance, which captures how distinctly a neuron’s activation distributions vary across concepts. Using Gemma-2-2B and multiple SAE variants across five benchmarks, we show that SAEs reduce polysemanticity and achieve higher concept separability. However, greater sparsity of SAEs does not always yield better separability and often impairs downstream performance. To assess practical utility, we evaluate concept-level interventions using two strategies: full neuron masking and partial suppression. We find that, compared to base models, SAEs enable more precise concept-level control when using partial suppression. Building on this, we propose Attenuation via Posterior Probabilities (APP), a new intervention method that uses concept-conditioned activation distributions for targeted suppression. APP outperforms existing approaches in targeted concept removal.

## Introduction

Large language models (LLMs) have achieved remarkable performance across a wide range of natural language tasks, often matching or surpassing human-level performance (Luo et al. 2025; Achiam et al. 2023; Touvron et al. 2023; Guo et al. 2025; Eslamian and Cheng 2025). Nonetheless, understanding how these models internally represent and manipulate concepts remains a major challenge. A key obstacle is polysemanticity: the phenomenon where individual neurons respond to multiple, semantically distinct concepts rather than encoding single, interpretable features (Janiak, Mathwin, and Heimersheim 2023; Olah, Mordvintsev, and Schubert 2017; Nguyen, Yosinski, and Clune 2016). This entanglement complicates the interpretation and analysis of model behavior, posing a significant barrier to building transparent and controllable AI systems (Sharkey et al. 2025; Marshall and Kirchner 2024; Bereska and Gavves 2024).

Dictionary learning via sparse autoencoders (SAEs) (Huben et al. 2024; Gao et al. 2025) has recently emerged as a promising approach to mitigating polysemanticity in neural representations. SAEs aim to transform dense activations of a desired component of the base LLM into sparse features by enforcing sparsity and encouraging each neuron to specialize in distinct, concept-specific features (Huben et al. 2024; Rajamanoharan et al. 2024a,b; Gao et al. 2025). The goal is to produce monosemantic representations, where individual neurons respond to single, well-defined concepts (Huben et al. 2024; Rajamanoharan et al. 2024a,b; Gao et al. 2025). The underlying hypothesis is intuitive: if we can force the model to use fewer neurons simultaneously, each active neuron should correspond to a more distinct and interpretable concept. Empirical studies have shown that SAEs can uncover interpretable features across domains such as vision and language, facilitating improved interpretability (Shu et al. 2025; Huben et al. 2024; Pach et al. 2025).

However, most of the evidence for the interpretability benefits of SAEs is qualitative, relying on case studies or anecdotal neuron visualizations, offering limited insight into their systematic effectiveness (Kissane et al. 2024; Li et al. 2025). While SAEs have higher computational costs and degraded downstream performance compared to their dense counterparts (Huben et al. 2024), no work has quantitatively compared their internal representations for monosemanticity: a core requirement for enhancing model interpretability. Without such comparison, the practical and theoretical value of sparsity remains poorly understood.

In this work, we conduct a systematic investigation into the effectiveness of SAEs in promoting monosemanticity in the internal representations of LLMs. In contrast to prior work that evaluates SAEs in isolation, we compare their representations to those of the corresponding base models, providing the first quantitative assessment of how sparsity affects concept disentanglement. Particularly, we conduct comprehensive evaluations using Gemma-2-2B (Rivière et al. 2024) and various SAEs of different widths and sparsity levels using five benchmark datasets. We begin by quantifying polysemanticity using overlap statistics, measuring the fraction of salient neurons that respond to multiple, semantically distinct concepts. While SAEs exhibit lower polysemanticity than their base models, this

overlap-based analysis remains coarse-grained: it treats all neurons that respond to multiple concepts as equally entangled, without considering how their activations vary across those concepts. In practice, a neuron may activate for several concepts, yet do so with clearly distinct activation distributions, suggesting behavior that may still be considered monosemantic. That is, monosemanticity is not solely about binary activation overlap, but rather about the separability of a neuron’s activation distributions across concepts.

We formalize this view by introducing a new concept separability score, based on the Jensen–Shannon distance (Lin 1991). This fine-grained, distribution-aware metric quantifies how well a neuron’s activations separate across different concepts by measuring the distance between their activation distributions. Using this score, we find that SAEs exhibit higher concept separability than their dense counterparts. Interestingly, we also observe that increasing sparsity does not always lead to better separability, and often comes at the cost of degraded downstream performance.

To further evaluate the practical utility of monosemantic representations of SAEs, we examine their effectiveness in enabling concept-level model interventions. Specifically, we assess how precisely concept-related behavior can be suppressed in SAEs compared to base models. We evaluate two intervention strategies: full neuron masking, which suppresses all activations of salient neurons associated with a target concept, and partial suppression, which intervenes in activations selectively based on their distributional association with the concept. Across SAEs and the base model, partial suppression outperforms full masking in most cases, achieving more effective suppression of the target concept while better preserving unrelated model behavior. Furthermore, our results show that SAEs support more precise and effective concept removal than their dense counterparts when applying partial suppression methods. These findings reinforce the idea that concept separability, when defined in terms of activation distributions rather than binary activation overlap, offers better model control and interpretability.

Additionally, motivated by the varying separability of concept activations across neurons, we introduce Attenuation via Posterior Probabilities (APP), a new intervention method that leverages concept-conditioned activation distributions to selectively suppress target concepts with minimal side effects. Specifically, APP computes the posterior probability that a given activation corresponds to a target concept and attenuates it accordingly. Among all methods evaluated, APP achieves the strongest and most targeted concept removal across both SAEs and base models.

In summary, this work makes the following contributions:

- We present the first quantitative analysis of monosemantic representations in SAEs relative to their base LLM.
- We introduce a concept separability score, based on the Jensen–Shannon distance, a fine-grained, distribution-aware metric that captures how well neuron activations separate for different concepts.
- We propose a new intervention method, a minimally invasive concept erasure technique, outperforming existing methods in both precision and side-effect minimization.

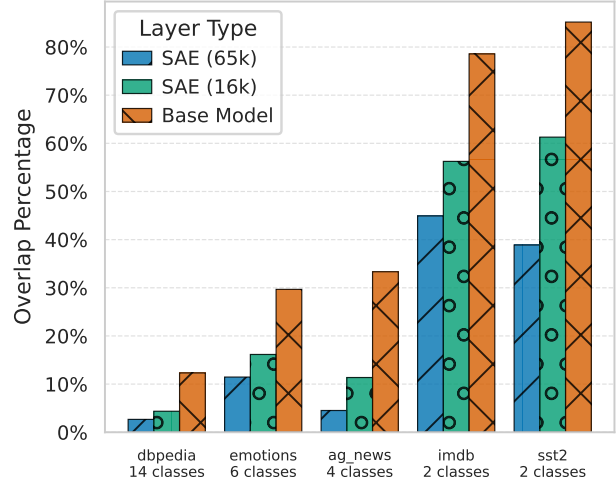


Figure 1: SAEs reduce neuron overlap in comparison to the base model, indicating lower polysemanticity. Higher-capacity SAEs (65k) further reduce overlap, suggesting more effective assignment of distinct neurons to separate concepts.

## Preliminaries

**Neuron.** A neuron refers to a component of a hidden state vector in a transformer layer. Given a hidden state  $h^l \in \mathbb{R}^d$  at layer  $l$ , the  $j$ -th neuron is denoted by  $h_j^l$ .

**Concept.** A concept  $c_i \in C$  is a semantic category assigned to each input (or its components), where  $C = c_1, \dots, c_k$ . For instance, sentence types (e.g., declarative, interrogative) or word-level tags (e.g., noun, verb) can serve as concepts. We focus on sentence-level concepts with one label per input.

**Datasets and Models.** We use five datasets: IMDB (Maas et al. 2011), AG News (Zhang, Zhao, and LeCun 2015), Emotions (Saravia et al. 2018), DBpedia (Zhang, Zhao, and LeCun 2015), and SST-2 (Socher et al. 2013). Our analysis is based on the Gemma-2-2B language model (Rivière et al. 2024) and several Sparse Autoencoders (SAEs) from GemmaScope (Lieberum et al. 2024).

## Analyzing Polysemanticity in SAEs

A neuron is considered polysemantic when it responds to multiple, distinct concepts rather than a single, well-defined one. Several studies have demonstrated that such polysemantic behavior is common in neural networks (Elhage et al. 2022; Bau et al. 2017; Scherlis et al. 2022; Lecomte et al. 2024; Marshall and Kirchner 2024; Olah, Mordvintsev, and Schubert 2017; Nguyen, Yosinski, and Clune 2016). This polysemanticity reduces the interpretability of models, motivating the development of Sparse Autoencoders (SAEs) (Huben et al. 2024; Rajamanoharan et al. 2024a,b; Gao et al. 2025). SAEs are designed to encourage sparsity in neural activations, aiming to align each neuron with a specific, distinct concept and thereby promote monosemanticity and interpretability. In the following, we quantitatively evaluate SAEs to better understand their effectiveness in improving monosemanticity.

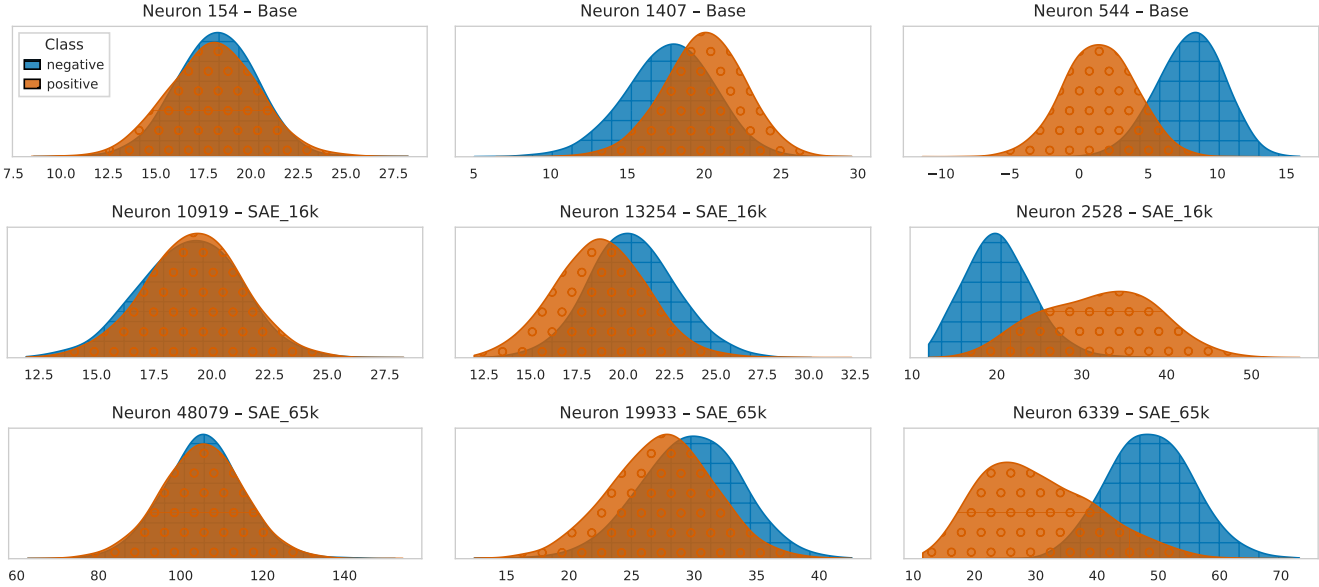


Figure 2: Across base model and SAEs (SAE-16k, SAE-65k), neurons exhibit varying degrees of separability in their activations. Some have completely overlapping activations across concepts, others show partial or clear separation. This variability underscores the importance of using distribution-aware metrics when assessing neuron monosemanticity.

### Salient Neuron Overlap

As a first step, we quantify polysemanticity by measuring the overlap percentage of salient neurons (i.e., neurons with high mean activation) across concepts. Specifically, for each concept, we identify the top 50 salient neurons by mean activation. Then, the overlap percentage is computed as the intersection-over-union of these top-K sets across concepts. This metric captures the extent to which neurons are shared across concepts, reflecting shared saliency and polysemanticity. The Figure 1 compares this shared saliency for the base model and two Sparse Autoencoders (SAEs) with different latent dimensions (16k and 65k), while maintaining comparable sparsity levels (116 vs. 93 active neurons). In the DBpedia dataset, we observe that nearly 12% of the top-activated (salient) neurons in the base model are shared across all 14 concepts. On the other hand, for the IMDB and SST-2 datasets, this percentage is considerably higher as these datasets contain only two concepts, which increases the likelihood that salient neurons are shared across both. Moreover, the Figure 1 confirms that SAEs exhibit reduced conceptual overlap, suggesting less polysemanticity; however, polysemantic neurons are still present. For example, in the AG News dataset, the percentage of shared salient neurons drops from around 30% in the base model to approximately 10% in the SAE with 16k dimensions. This is still a relatively high percentage, indicating that over 10% of the most salient neurons are shared across all four concepts. Moreover, another notable observation is that the 65k-dimensional SAEs exhibit lower polysemanticity than their 16k-dimensional counterparts across all datasets. This reinforces the idea that larger SAEs have greater capacity to allocate distinct neurons to specific concepts, thereby enhancing interpretability. For additional analysis evaluating all active SAE neurons, not just the top 50, see Appendix E.

### SAEs Activation Distributions

So far, we have analyzed polysemanticity by quantifying neuron overlap based on activation frequency, specifically, how often a neuron is active or salient across different concepts. While these approaches offer useful aggregate insights, they treat neuron activation as a binary or averaged signal, overlooking the distributional characteristics of how neurons respond to each concept. In other words, a neuron might be shared across multiple concepts, but the manner in which it activates for each could vary significantly, ranging from broad, overlapping responses to distinct, well-separated patterns. To better capture this nuance, Figure 2 displays the full activation distributions of selected neurons across concept classes in the IMDB dataset, comparing the base model with two SAE variants of differing capacities. We include an analogous visualization for the AG News dataset in Appendix A.

These plots reveal two key patterns: (1) consistent with prior observations (Haider et al. 2025), neuron activations in both the base model and SAEs tend to follow approximately Gaussian distributions; and (2) while some neurons are shared across multiple concepts, their activation distributions can range from highly overlapping to clearly separable. This underscores a fundamental limitation of mean-based or binary overlap measurements, which can overlook meaningful distinctions in activation behavior. To more accurately measure polysemanticity, it is therefore necessary to employ a metric that captures the full shape of activation distributions across concepts. To this end, we introduce a new concept separability score, based on the Jensen-Shannon distance, which quantifies the degree of separation between concept-specific activation distributions.

**Concept Separability Score.** To quantify how separable a

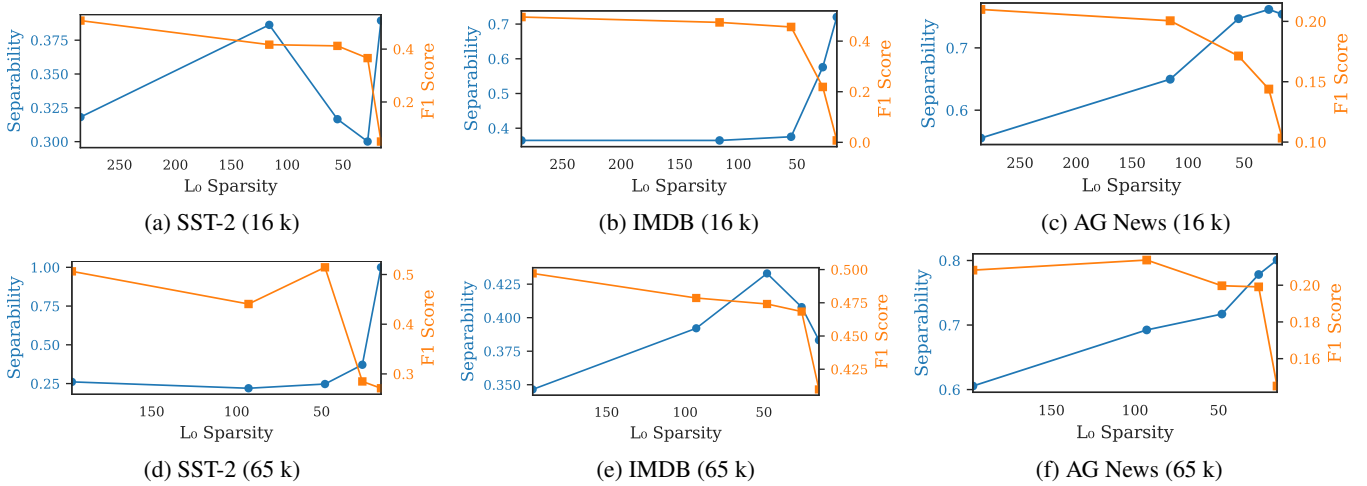


Figure 3: While increased sparsity generally enhances concept separability, excessive sparsity can sometimes lead to a significant drop in separability.

|                        | IMDB         | AG News      | Emotions     | DBpedia      | SST2         |
|------------------------|--------------|--------------|--------------|--------------|--------------|
| Base                   | 0.259        | 0.339        | 0.296        | 0.405        | 0.183        |
| SAE (width_16k/10.116) | 0.364        | 0.649        | <b>0.431</b> | 0.621        | <b>0.386</b> |
| SAE (width_65k/10.93)  | <b>0.392</b> | <b>0.692</b> | 0.427        | <b>0.680</b> | 0.219        |

Table 1: Separability Score  $S$  across datasets.

neuron's activation distributions are across  $k$  concepts, let

$$f_{h_j^l|c_i}(x) = p(h_j^l = x | c_i), \quad i = 1, \dots, k,$$

and define the mixture

$$M^{(l,j)}(x) = \frac{1}{k} \sum_{i=1}^k f_{h_j^l|c_i}(x).$$

We then define the standard Jensen–Shannon divergence (Lin 1991) as

$$\text{JSD}(f_{h_j^l|c_1}, \dots, f_{h_j^l|c_k}) = H(M^{(l,j)}) - \frac{1}{k} \sum_{i=1}^k H(f_{h_j^l|c_i}).$$

Next, we normalize to get a distance in  $[0, 1]$ :

$$D_{\text{JS}}(f_{h_j^l|c_1}, \dots, f_{h_j^l|c_k}) = \frac{\sqrt{\text{JSD}(f_{h_j^l|c_1}, \dots, f_{h_j^l|c_k})}}{\sqrt{\log_2 k}},$$

Moreover, we assign  $D_{\text{JS}} = 1$  whenever a neuron's activations are all attributed to a single concept. Finally, the layer-level separability is

$$S^l = \frac{1}{d} \sum_{j=1}^d D_{\text{JS}}(f_{h_j^l|c_1}, \dots, f_{h_j^l|c_k}),$$

where  $d$  is the number of neurons in layer  $l$ .

Table 1 reports the concept separability score  $S \in [0, 1]$  for layer 25, where higher values reflect more distinct activation distributions across concepts, indicating greater

monosemanticity. Across all five datasets, both Sparse Autoencoders (SAEs) substantially improve separability compared to the base model. For example, on DBpedia (14 classes), the score rises from 0.405 in the base model to 0.621 and 0.680 for SAEs with 16 K and 65 K dimensions respectively, an increase of over 50%.

In most cases, increasing SAE capacity yields higher separability, consistent with the idea that more expressive latent spaces better disentangle concepts. However, two exceptions emerge. On SST2, separability actually decreases when moving from 16 K to 65 K dimensions. A similar, though smaller, decline is observed in the Emotions dataset.

## Impact of SAE Sparsity

With our new separability score, we investigate two key questions: (1) Does increasing SAE sparsity (i.e., reducing the  $L_0$  norm) consistently improve concept separability and thus, interpretability? (2) Does increasing sparsity also lead to a consistent drop in model performance? To address these questions, we present Figure 3, which illustrates how the separability score  $S \in [0, 1]$  (a proxy for interpretability) and the F1 score vary with increasing SAE sparsity.

**Effect of Sparsity on Concept Separability.** As shown in Figure 3, concept separability usually increases with greater sparsity, indicating improved interpretability. However, interestingly, at some points, excessive sparsity can degrade separability. For instance, in the SST-2 dataset (subplot (a)), the separability score drops by 18.06% when the number of active neurons ( $L_0$  norm) is decreased from 116 to 55. A similar trend appears in the IMDB dataset (subplot (e)), with an 11.50% drop as the number of active neurons decreases from 48 to 15. A smaller decline is also observed in AG News (subplot (c)).

**Effect of Sparsity on Model Performance.** Increasing SAE sparsity by reducing the number of active neurons, generally makes reconstruction harder, leading to lower F1 scores in most cases. Interestingly, however, greater sparsity occasionally yields slight performance gains. For instance, in the

SST-2 dataset (subplot (d), Figure 3), the F1 score improves by 16.74% as the number of active neurons decreases from 93 to 48 ( $L_0 = 93$  to  $L_0 = 48$ ).

Our analysis focused on the final transformer layer of the Gemma model (layer 25). To ensure the robustness of our findings, we repeated the experiments on layer 24 and observed similar patterns; see Appendix D.

Building on our finding that sparse autoencoders yield more separable concept representations, we next assess whether this improved separability enables more precise concept erasure interventions.

## Concept Erasure

Concept erasure encompasses interventions that aim to remove a specific concept from a model’s internal representation, ideally without affecting other concepts (Dalvi et al. 2019a,b; Dai et al. 2022; Morcos et al. 2018). Formally, let  $M$  be a trained model that maps an input  $x$  to a concept label  $M(x) = c$ . An ideal erasure yields a modified model  $M'_{\text{ideal}}$  satisfying:

$$M'_{\text{ideal}}(x) = \begin{cases} \neq M(x), & \text{if } M(x) = c, \\ = M(x), & \text{if } M(x) \neq c. \end{cases}$$

That is, the model should unlearn the target concept  $c$  while preserving its behavior on all other concepts.

As shown in Figure 2, some neurons exhibit considerable overlap in their activation distributions across concepts, while others show separability. This pattern appears in both the base model and SAEs, suggesting that concept erasure techniques should not treat all activation values in one neuron identically. Instead, we propose a more targeted approach that considers where an activation falls within the distribution. Specifically, values in regions uniquely tied to a concept (i.e., those regions of distribution that are clearly separable from other concepts) should be suppressed more strongly, while those shared across concepts should be damped more conservatively to preserve other concepts. To achieve this, we introduce Attenuation via Posterior Probabilities (APP), which modulates suppression based on distributional separability.

## Attenuation via Posterior Probabilities (APP)

Given all neurons  $h_j^l$  of layer  $l$ , with individual activations  $x_j^l$  for  $j = 1, \dots, d$ , and a target concept  $c_i \in C$ , our goal is to selectively suppress the activation  $x_j^l$  that is attributable to  $c_i$ , while preserving contributions from other concepts.

We begin by computing the posterior probability that a given activation  $x_j^l$  arose from concept  $c_i$ , under the assumption that all concepts are a priori equally likely:

$$\begin{aligned} \pi_{j,i}(x_j^l) &= p(c_i \mid h_j^l = x_j^l) = \frac{p(h_j^l = x_j^l \mid c_i) p(c_i)}{\sum_{m=1}^k p(h_j^l = x_j^l \mid c_m) p(c_m)}, \\ &= \frac{p(h_j^l = x_j^l \mid c_i)}{\sum_{m=1}^k p(h_j^l = x_j^l \mid c_m)} \equiv \frac{f_{h_j^l \mid c_i}(x_j^l)}{\sum_{m=1}^k f_{h_j^l \mid c_m}(x_j^l)}. \end{aligned}$$

By definition,  $\sum_{i=1}^k \pi_{j,i}(x_j^l) = 1$ .

To avoid unreliable posterior estimates from low-density regions, we limit our attention to the central region of the target concept’s activation distribution, where density estimates are more reliable. Let  $\mu_{j,i}$  and  $\sigma_{j,i}$  denote the mean and standard deviation of neuron  $h_j^l$  under concept  $c_i$ , and define the valid damping window as:

$$W_{j,i} = [\mu_{j,i} - 2.5 \sigma_{j,i}, \mu_{j,i} + 2.5 \sigma_{j,i}].$$

The damping factor  $\alpha_{j,i}(x)$  is then defined as:

$$\alpha_{j,i}(x) = \begin{cases} 1 - \pi_{j,i}(x), & x \in W_{j,i}, \\ 1, & \text{otherwise.} \end{cases}$$

With  $\alpha \approx 0$  when  $x$  is very typical of the target concept  $c_i$ . Finally, we apply this factor to dampen the activation:

$$\tilde{x}_j^l = \alpha_{j,i}(x_j^l) x_j^l = \begin{cases} [1 - \pi_{j,i}(x_j^l)] x_j^l, & |x_j^l - \mu_{j,i}| \leq 2.5 \sigma_{j,i}, \\ x_j^l, & \text{otherwise.} \end{cases}$$

This formulation enables precise, concept-aware suppression while leaving unrelated or uncertain activations unchanged.

## Baseline Methods

We compare our concept erasure approach with the following baselines:

**AURA (Suau et al. 2024):** Ranks neurons by AUROC, selects those with  $\text{AUROC} > 0.5$ , and dampens each output  $z_m$  by  $\alpha_m$  (0 for perfect classifiers, 1 for random), removing concept signals without hyperparameters.

**Range Masking (Haider et al. 2025):** Identifies concept-relevant neurons and suppresses activations within their typical range ( $\mu \pm 2.5\sigma$ ), erasing concept-specific signals while preserving others.

**Adaptive Dampening (Haider et al. 2025):** Identifies concept-relevant neurons and dampens activations in proportion to their distance from the concept mean, (strongly near the mean, minimally farther away), enabling precise concept removal.

**Full Masking (Dalvi et al. 2019a; Dai et al. 2022):** A simple baseline where all neurons associated with the target concept are completely zeroed out to eliminate the concept from the representation.

## Metrics

We evaluate the causal effect of our interventions using three metrics: task accuracy, predictive confidence, and perplexity.

Accuracy and confidence are measured both before and after intervention, for the target concept  $c$  and all auxiliary concepts  $c' \neq c$ . The goal is to assess how much the intervention selectively affects the target concept while minimizing disruption to others.

Let  $D_{\text{Acc}}$  denote the drop in accuracy for the target concept, and  $D'_{\text{Acc}}$  the average drop in accuracy across auxiliary concepts. Similarly, let  $D_{\text{Conf}}$  and  $D'_{\text{Conf}}$  be the drops in predictive confidence for the target and auxiliary concepts, respectively.

Table 2: Concept Erasure Results by Type/Method across datasets (Gemma)

| Type                         | Method   | IMDB                           |                                 |                   | AG News                        |                                 |                   | Emotions                       |                                 |                   | DBpedia                        |                                 |                   | SST2                           |                                 |                   |
|------------------------------|----------|--------------------------------|---------------------------------|-------------------|--------------------------------|---------------------------------|-------------------|--------------------------------|---------------------------------|-------------------|--------------------------------|---------------------------------|-------------------|--------------------------------|---------------------------------|-------------------|
|                              |          | $\Delta_{\text{Acc}} \uparrow$ | $\Delta_{\text{Conf}} \uparrow$ | DPPL $\downarrow$ | $\Delta_{\text{Acc}} \uparrow$ | $\Delta_{\text{Conf}} \uparrow$ | DPPL $\downarrow$ | $\Delta_{\text{Acc}} \uparrow$ | $\Delta_{\text{Conf}} \uparrow$ | DPPL $\downarrow$ | $\Delta_{\text{Acc}} \uparrow$ | $\Delta_{\text{Conf}} \uparrow$ | DPPL $\downarrow$ | $\Delta_{\text{Acc}} \uparrow$ | $\Delta_{\text{Conf}} \uparrow$ | DPPL $\downarrow$ |
| Base                         | APP      | <b>0.377</b>                   | <b>0.194</b>                    | 0.569             | <b>0.335</b>                   | <b>0.257</b>                    | <b>0.378</b>      | <b>0.045</b>                   | 0.089                           | <b>0.154</b>      | 0.113                          | <b>0.104</b>                    | <b>0.076</b>      | <b>0.274</b>                   | <b>0.121</b>                    | <b>0.307</b>      |
|                              | Aura     | -0.038                         | -0.023                          | 2.419             | 0.070                          | 0.089                           | 1.789             | -0.021                         | 0.0002                          | 1.932             | 0.092                          | 0.064                           | 2.792             | -0.120                         | -0.035                          | 0.553             |
|                              | Range    | 0.066                          | 0.033                           | <b>0.511</b>      | 0.064                          | 0.087                           | 1.057             | 0.029                          | <b>0.100</b>                    | 0.797             | <b>0.168</b>                   | <b>0.109</b>                    | 0.700             | 0.079                          | 0.030                           | 0.402             |
|                              | Adaptive | 0.106                          | 0.048                           | <b>0.287</b>      | 0.046                          | 0.082                           | <b>0.561</b>      | 0.028                          | 0.081                           | <b>0.436</b>      | 0.120                          | 0.099                           | <b>0.387</b>      | 0.030                          | 0.023                           | <b>0.225</b>      |
|                              | Full     | 0.023                          | 0.012                           | 9.692             | <b>0.070</b>                   | 0.070                           | 16.574            | <b>0.032</b>                   | <b>0.107</b>                    | 16.913            | <b>0.169</b>                   | 0.102                           | 10.922            | <b>0.124</b>                   | <b>0.030</b>                    | 38.469            |
| SAE<br>width: 65k<br>l0: 93  | APP      | <b>0.596</b>                   | <b>0.296</b>                    | <b>0.140</b>      | 0.603                          | <b>0.441</b>                    | <b>0.232</b>      | 0.238                          | <b>0.275</b>                    | <b>0.058</b>      | <b>0.399</b>                   | <b>0.219</b>                    | <b>0.114</b>      | 0.642                          | <b>0.238</b>                    | <b>0.057</b>      |
|                              | Aura     | 0.322                          | 0.208                           | 0.266             | 0.588                          | <b>0.365</b>                    | 0.575             | <b>0.330</b>                   | <b>0.299</b>                    | 0.256             | 0.357                          | <b>0.213</b>                    | 0.490             | <b>0.650</b>                   | 0.176                           | 0.164             |
|                              | Range    | 0.050                          | 0.018                           | 0.276             | 0.588                          | 0.121                           | 0.554             | 0.143                          | 0.023                           | 0.387             | 0.252                          | 0.056                           | 0.446             | 0.026                          | 0.007                           | 0.192             |
|                              | Adaptive | 0.135                          | 0.066                           | <b>0.169</b>      | 0.594                          | 0.209                           | <b>0.366</b>      | 0.180                          | 0.080                           | 0.203             | 0.222                          | 0.083                           | <b>0.279</b>      | 0.074                          | 0.029                           | 0.109             |
|                              | Full     | 0.002                          | 0.0001                          | 2.238             | <b>0.606</b>                   | 0.006                           | 4.755             | 0.118                          | 0.001                           | 5.441             | 0.275                          | 0.018                           | 3.892             | 0.000                          | 0.000001                        | 4.030             |
| SAE<br>width: 16k<br>l0: 116 | APP      | 0.484                          | 0.242                           | <b>0.293</b>      | 0.584                          | <b>0.369</b>                    | <b>0.571</b>      | 0.267                          | <b>0.269</b>                    | <b>0.174</b>      | <b>0.312</b>                   | <b>0.152</b>                    | <b>0.140</b>      | <b>0.446</b>                   | <b>0.235</b>                    | <b>0.762</b>      |
|                              | Aura     | <b>0.548</b>                   | <b>0.247</b>                    | 0.420             | <b>0.598</b>                   | 0.284                           | 1.252             | <b>0.325</b>                   | <b>0.281</b>                    | 0.450             | 0.257                          | <b>0.140</b>                    | 0.836             | 0.083                          | 0.168                           | 1.375             |
|                              | Range    | 0.099                          | 0.004                           | 0.454             | 0.357                          | 0.118                           | 0.886             | 0.096                          | 0.009                           | 0.445             | 0.208                          | 0.053                           | 0.446             | 0.274                          | 0.009                           | 0.839             |
|                              | Adaptive | 0.124                          | 0.021                           | <b>0.308</b>      | 0.360                          | 0.172                           | <b>0.680</b>      | 0.123                          | 0.044                           | <b>0.291</b>      | 0.177                          | 0.071                           | <b>0.288</b>      | 0.272                          | 0.029                           | <b>0.778</b>      |
|                              | Full     | 0.002                          | 0.000005                        | 5.271             | 0.322                          | 0.006                           | 6.474             | 0.044                          | 0.0004                          | 6.642             | 0.187                          | 0.0007                          | 5.639             | 0.000                          | 0.0000001                       | 5.447             |
| SAE<br>width: 65k<br>l0: 197 | APP      | <b>0.618</b>                   | <b>0.305</b>                    | <b>0.317</b>      | <b>0.612</b>                   | <b>0.447</b>                    | <b>0.411</b>      | 0.247                          | 0.283                           | <b>0.307</b>      | <b>0.362</b>                   | <b>0.235</b>                    | <b>0.083</b>      | 0.738                          | <b>0.295</b>                    | <b>0.095</b>      |
|                              | Aura     | <b>0.397</b>                   | <b>0.197</b>                    | 0.377             | <b>0.611</b>                   | <b>0.391</b>                    | 0.873             | <b>0.304</b>                   | <b>0.317</b>                    | <b>0.456</b>      | <b>0.297</b>                   | <b>0.235</b>                    | 0.596             | <b>0.767</b>                   | <b>0.233</b>                    | 0.145             |
|                              | Range    | 0.026                          | 0.012                           | 0.460             | 0.294                          | 0.046                           | 0.756             | 0.128                          | 0.021                           | 0.615             | 0.292                          | 0.106                           | 0.335             | 0.005                          | 0.0008                          | 0.148             |
|                              | Adaptive | 0.114                          | 0.069                           | <b>0.345</b>      | 0.295                          | 0.108                           | <b>0.552</b>      | 0.169                          | 0.104                           | 0.466             | 0.257                          | <b>0.147</b>                    | <b>0.205</b>      | 0.019                          | 0.014                           | 0.109             |
|                              | Full     | 0.008                          | 0.0007                          | 4.179             | 0.268                          | 0.0005                          | 7.490             | 0.086                          | 0.002                           | 6.844             | 0.216                          | 0.019                           | 6.203             | 0                              | 0.00002                         | 3.599             |
| SAE<br>width: 16k<br>l0: 285 | APP      | 0.314                          | 0.121                           | <b>0.658</b>      | <b>0.628</b>                   | <b>0.355</b>                    | <b>0.877</b>      | 0.210                          | <b>0.221</b>                    | <b>0.424</b>      | <b>0.274</b>                   | <b>0.147</b>                    | <b>0.167</b>      | 0.043                          | 0.046                           | <b>0.628</b>      |
|                              | Aura     | <b>0.570</b>                   | <b>0.239</b>                    | 0.780             | <b>0.551</b>                   | 0.340                           | 1.628             | <b>0.269</b>                   | <b>0.293</b>                    | <b>0.649</b>      | 0.158                          | <b>0.111</b>                    | 0.975             | <b>0.827</b>                   | <b>0.201</b>                    | 0.648             |
|                              | Range    | 0.016                          | 0.004                           | 0.978             | 0.447                          | 0.064                           | 1.886             | 0.108                          | 0.011                           | 1.350             | <b>0.181</b>                   | 0.057                           | 0.958             | 0.047                          | 0.0007                          | 0.969             |
|                              | Adaptive | 0.027                          | 0.021                           | <b>0.717</b>      | 0.429                          | 0.142                           | <b>1.331</b>      | 0.117                          | 0.067                           | 0.895             | 0.145                          | 0.083                           | <b>0.582</b>      | 0.023                          | 0.004                           | 0.746             |
|                              | Full     | 0.00008                        | 0.00005                         | 6.646             | 0.140                          | 0.0003                          | 16.285            | 0.056                          | 0.001                           | 8.082             | 0.153                          | 0.023                           | 9.510             | 0.009                          | 0.000005                        | 7.479             |

Using these, we compute two scores:

$$\Delta_{\text{Acc}} = D_{\text{Acc}} - D'_{\text{Acc}}, \quad \Delta_{\text{Conf}} = D_{\text{Conf}} - D'_{\text{Conf}}.$$

Higher values of  $\Delta_{\text{Acc}}$  and  $\Delta_{\text{Conf}}$  indicate more precise interventions, strongly affecting the target concept while preserving performance on others. In the main text, we report only  $\Delta_{\text{Acc}}$  and  $\Delta_{\text{Conf}}$ ; the full metric breakdowns are included in Appendix C.

Lastly, to capture the overall impact on the model’s generative ability, we measure the drop in perplexity:

$$\text{DPPL} = \text{PPL}_{\text{base}} - \text{PPL}_{\text{post}}.$$

## Implementation Details

To estimate the densities  $f_{h_j^l | c_i}(x_j^l)$  required by APP, we use kernel density estimation (KDE). Since naive KDE is computationally expensive, we implement a histogram-based approximation that significantly improves efficiency with minimal impact on accuracy. Full implementation details, including runtime complexity, are provided in Appendix B.

Moreover, Range Masking, Adaptive Dampening, and Full Masking each rely on a saliency threshold, which is a hyperparameter that selects the top- $p\%$  of neurons deemed most relevant to the target concept. We set  $p = 0.1$  for IMDB,  $p = 0.3$  for AG News, and  $p = 0.2$  for the remaining datasets. In contrast, AURA (Suau et al. 2024) and our method, APP, do not require this hyperparameter. Both apply interventions across all neurons in the selected layer, avoiding the need to tune or justify a saliency cutoff. However, because SAE neurons typically activate on only a small subset of inputs for any given concept, we introduce an activation-frequency threshold  $\tau$  to ensure reliability. Specifically, for each SAE neuron  $h_j^l$ , and each concept  $c_i$ , let  $\mathcal{X}_{c_i}$  be the set of corresponding input samples. We define the firing frequency of  $h_j^l$  on  $c_i$  as

$$f_{j,i} = \frac{|\{x \in \mathcal{X}_{c_i} : h_j^l(x) > 0\}|}{|\mathcal{X}_{c_i}|}.$$

We exclude neuron  $h_j^l$  from all concept-erasure methods if  $f_{j,i} < \tau$ , as sparse activations preclude meaningful intervention. In all experiments, we set  $\tau = 0.1$ .

We apply all interventions at a consistent computation point, immediately before the language-model head, ensuring comparability across models and methods. Specifically, we intervene after the MLP and residual-stream addition in the final transformer block of the model. For SAEs, we apply interventions just after the SAE’s activation nonlinearity.

To isolate the causal impact on prediction, interventions are restricted to the token corresponding to the model’s output label. This allows us to precisely assess the influence of each concept-erasure method on the final decision, without confounding effects from earlier tokens.

## Results and Analysis

**Comparison of Intervention Effectiveness: SAEs vs. Base Model.** As it can be seen in Table 2, across nearly all settings, we find that partial intervention methods (particularly APP and Aura) consistently achieve higher  $\Delta_{\text{Acc}}$  and  $\Delta_{\text{Conf}}$  when applied to SAE representations compared to the base model. Specifically, for APP, SAE-based interventions outperformed the base model in 36 out of 40 comparisons. For Aura, SAE-based interventions were more effective in all 40 cases. In contrast, full masking shows little benefit from SAE representations: only 11 out of 40 interventions resulted in better outcomes than when applied to the base model. This discrepancy suggests that coarse suppression methods fail to capitalize on the increased concept separability offered by SAEs. These findings reinforce that SAE representations are more disentangled and that fine-grained, distribution-aware methods are better equipped to exploit this structure for effective concept removal. Furthermore, focusing specifically on the APP intervention (which is a partial intervention), we observe that within the SAE family, increasing capacity consistently enhances interven-

tion quality. In particular,  $\Delta_{\text{Conf}}$  consistently increases as we scale from 16k to 65k latent dimensions, reflecting improved confidence suppression for the target concept.  $\Delta_{\text{Acc}}$  also improves across most datasets, with only minor exceptions, further underscoring the role of latent dimensionality in enabling more precise and effective concept removal.

**Partial Interventions Vs Full Interventions.** Full masking ranks as the worst-performing method in 36 out of 40  $\Delta$ -metrics on the SAEs and in 1 out of 10  $\Delta$ -metrics on the base model, and it also produces the largest perplexity drop in all DPPL evaluations across SAEs and the base model. This underscores that distribution-aware partial methods (e.g., APP, AURA), which leverage activation distributions, are far more effective for targeted concept removal than the coarse, distribution-agnostic full-masking approach.

**APP Outperforms Baselines in Concept Erasure.** Among concept erasure techniques, the APP method (our proposed approach) and Aura consistently achieve the best results across both evaluation metrics:  $\Delta_{\text{Acc}}$  and  $\Delta_{\text{Conf}}$ . For  $\Delta_{\text{Acc}}$ , in the 25 comparisons (5 datasets  $\times$  5 types), APP achieves the top performance in 13 cases, with Aura close behind in 10 cases. For  $\Delta_{\text{Conf}}$ , APP again outperforms all other methods in 16 out of 25 experiments, while Aura comes first in 8. These results underscore the robustness of APP: it effectively removes the target concept while having a minimal unintended impact on other concepts. Table 2 further reports the change in perplexity ( $\Delta_{\text{PPL}}$ ) across datasets, serving as a proxy for the model’s overall language-modeling performance after concept removal. In all experiments except two, APP achieves the smallest  $\Delta_{\text{PPL}}$ , demonstrating that it preserves Gemma’s predictive fluency more effectively, and is therefore the least disruptive, among the erasure methods. The Adaptive method performs second best in most cases, showing the next smallest drop in perplexity after APP.

**Comparative Analysis of APP and AURA.** The superior effectiveness of AURA and APP on both  $\Delta_{\text{Acc}}$  and  $\Delta_{\text{Conf}}$  stems from the fact that they explicitly model not only the target-concept distribution but also the distributions of all auxiliary concepts. By calibrating their interventions to maximize disruption of  $c$  while minimizing collateral effects on  $c' \neq c$ , both methods achieve higher  $\Delta$  values than approaches that consider only the target distribution. Between these two, APP pulls ahead of AURA because it leverages fine-grained, activation-specific damping rather than a single, per-neuron factor. AURA mutes an “expert” neuron uniformly, regardless of whether a particular activation is highly characteristic of the target concept, whereas APP computes  $\pi_{j,i}(x)$  for each activation and suppresses only the portions of the distribution uniquely associated with  $c_i$ . This activation-aware attenuation not only sharpens concept removal (higher  $\Delta_{\text{Acc}}$  and  $\Delta_{\text{Conf}}$ ) but also preserves the model’s overall fluency more effectively (smaller  $\Delta_{\text{PPL}}$ ).

## Related Works

### Sparse Autoencoders for Feature Discovery

Sparse Autoencoders (SAEs) have emerged as a powerful method for learning interpretable, monosemantic features from neural network activations (Huben et al. 2024). Recent

advances have focused on improving reconstruction quality and scaling through architectural and training strategy innovations such as JumpReLU activations, BatchTopK sparsity, gated, and end-to-end training frameworks (Rajamanoharan et al. 2024a,b; Gao et al. 2025; Bussmann, Leask, and Nanda 2024; Braun et al. 2024). Empirical analyses have validated SAEs’ ability to discover meaningful structures across different domains, from vision-language models to algorithmic patterns like temporal difference learning in LLMs (Sun et al. 2025b; Pach et al. 2025; Demircan et al. 2025). Moreover, evaluation studies have highlighted both their utility for interpretability tasks and remaining challenges with polysemantic representations (Kantamneni et al. 2025; Minegishi et al. 2025). *However, none of these empirical analyses evaluated the separability of activation distributions in SAEs as a measure of polysemanticity.*

### SAE-Based Model Control

The interpretable features learned by SAEs enable precise control over language model behavior. Several works have demonstrated effective steering by carefully selecting and manipulating SAE features, with approaches ranging from supervised methods for identifying relevant dimensions to frameworks using hypernetworks (Arad, Mueller, and Belinkov 2025; He et al. 2025a,b; Bayat et al. 2025; Sun et al. 2025a). *However, prior SAE-based control methods did not utilize posterior probabilities, limiting their precision.*

### Base Model Control and Causal Analysis

Complementing SAE-based approaches, researchers have developed techniques for direct activation control and causal analysis in the base language models. General frameworks for transporting activations facilitate intervention across model architectures (Rodriguez et al. 2025), while causal tracing methods enable precise localization and editing of specific knowledge or biases (Vig et al. 2020; Meng et al. 2022, 2023). These approaches offer foundational tools for probing and manipulating model behavior at the activation level. *However, again, they do not leverage posterior probabilities for better intervention and have been applied exclusively to base models, not to representations learned by SAEs.*

## Conclusion

This work presents the first quantitative analysis of monosemanticity in SAEs compared to their dense base models. We show that while SAEs reduce polysemanticity and improve concept separability, increased sparsity does not always enhance interpretability and often comes with trade-offs in downstream performance. To better characterize monosemanticity, we introduce an activation distribution-aware concept separability score based on the Jensen–Shannon distance, which captures fine-grained distinctions in neuron activations across concepts. We also demonstrate that SAEs support more precise concept-level interventions than base models, particularly when using partial suppression. Building on this, we propose a new method, Attenuation via Posterior Probabilities, which achieves more targeted and effective concept removal with minimal side effects.

## References

Achiam, J.; Adler, S.; Agarwal, S.; Ahmad, L.; Akkaya, I.; Aleman, F. L.; Almeida, D.; Altenschmidt, J.; Altman, S.; Anadkat, S.; et al. 2023. Gpt-4 technical report. *arXiv preprint arXiv:2303.08774*.

Arad, D.; Mueller, A.; and Belinkov, Y. 2025. SAEs Are Good for Steering—If You Select the Right Features. *arXiv preprint arXiv:2505.20063*.

Bau, D.; Zhou, B.; Khosla, A.; Oliva, A.; and Torralba, A. 2017. Network Dissection: Quantifying Interpretability of Deep Visual Representations. In *Computer Vision and Pattern Recognition*.

Bayat, R.; Rahimi-Kalahroudi, A.; Pezeshki, M.; Chandar, S.; and Vincent, P. 2025. Steering large language model activations in sparse spaces. *arXiv preprint arXiv:2503.00177*.

Bereska, L.; and Gavves, S. 2024. Mechanistic Interpretability for AI Safety - A Review. *Transactions on Machine Learning Research*. Survey Certification, Expert Certification.

Braun, D.; Taylor, J.; Goldowsky-Dill, N.; and Sharkey, L. 2024. Identifying Functionally Important Features with End-to-End Sparse Dictionary Learning. In *The Thirty-eighth Annual Conference on Neural Information Processing Systems*.

Bussmann, B.; Leask, P.; and Nanda, N. 2024. Batchtop sparse autoencoders. *arXiv preprint arXiv:2412.06410*.

Dai, D.; Dong, L.; Hao, Y.; Sui, Z.; Chang, B.; and Wei, F. 2022. Knowledge Neurons in Pretrained Transformers. In Muresan, S.; Nakov, P.; and Villavicencio, A., eds., *Proceedings of the 60th Annual Meeting of the Association for Computational Linguistics (Volume 1: Long Papers)*, 8493–8502. Dublin, Ireland: Association for Computational Linguistics.

Dalvi, F.; Durrani, N.; Sajjad, H.; Belinkov, Y.; Bau, A.; and Glass, J. 2019a. What is one grain of sand in the desert? analyzing individual neurons in deep NLP models. In *Proceedings of the Thirty-Third AAAI Conference on Artificial Intelligence and Thirty-First Innovative Applications of Artificial Intelligence Conference and Ninth AAAI Symposium on Educational Advances in Artificial Intelligence, AAAI’19/IAAI’19/EAAI’19*. AAAI Press. ISBN 978-1-57735-809-1.

Dalvi, F.; Nortonsmith, A.; Bau, A.; Belinkov, Y.; Sajjad, H.; Durrani, N.; and Glass, J. 2019b. NeuroX: A Toolkit for Analyzing Individual Neurons in Neural Networks. *Proceedings of the AAAI Conference on Artificial Intelligence*, 33(01): 9851–9852.

Demircan, C.; Saanum, T.; Jagadish, A. K.; Binz, M.; and Schulz, E. 2025. Sparse Autoencoders Reveal Temporal Difference Learning in Large Language Models. In *The Thirteenth International Conference on Learning Representations*.

Elhage, N.; Hume, T.; Olsson, C.; Schiefer, N.; Henighan, T.; Kravec, S.; Hatfield-Dodds, Z.; Lasenby, R.; Drain, D.; Chen, C.; Grosse, R.; McCandlish, S.; Kaplan, J.; Amodei, D.; Wattenberg, M.; and Olah, C. 2022. Toy Models of Superposition. *Transformer Circuits Thread*. [Https://transformer-circuits.pub/2022/toy\\_model/index.html](Https://transformer-circuits.pub/2022/toy_model/index.html).

Eslamian, A.; and Cheng, Q. 2025. TabNSA: Native Sparse Attention for Efficient Tabular Data Learning. *arXiv preprint arXiv:2503.09850*.

Gao, L.; la Tour, T. D.; Tillman, H.; Goh, G.; Troll, R.; Radford, A.; Sutskever, I.; Leike, J.; and Wu, J. 2025. Scaling and evaluating sparse autoencoders. In *The Thirteenth International Conference on Learning Representations*.

Guo, D.; Yang, D.; Zhang, H.; Song, J.; Zhang, R.; Xu, R.; Zhu, Q.; Ma, S.; Wang, P.; Bi, X.; et al. 2025. Deepseek-r1: Incentivizing reasoning capability in llms via reinforcement learning. *arXiv preprint arXiv:2501.12948*.

Haider, M. U.; Rizwan, H.; Sajjad, H.; Ju, P.; and Siddique, A. 2025. Neurons Speak in Ranges: Breaking Free from Discrete Neuronal Attribution. *arXiv preprint arXiv:2502.06809*.

He, Z.; Jin, M.; Shen, B.; Payani, A.; Zhang, Y.; and Du, M. 2025a. SAE-SSV: Supervised Steering in Sparse Representation Spaces for Reliable Control of Language Models. *arXiv preprint arXiv:2505.16188*.

He, Z.; Zhao, H.; Qiao, Y.; Yang, F.; Payani, A.; Ma, J.; and Du, M. 2025b. Saif: A sparse autoencoder framework for interpreting and steering instruction following of language models. *arXiv preprint arXiv:2502.11356*.

Huben, R.; Cunningham, H.; Smith, L. R.; Ewart, A.; and Sharkey, L. 2024. Sparse Autoencoders Find Highly Interpretable Features in Language Models. In *The Twelfth International Conference on Learning Representations*.

Janiak, J.; Mathwin, C.; and Heimersheim, S. 2023. Polysemantic Attention Head in a 4-Layer Transformer. <https://www.lesswrong.com/posts/nJFTS5iiJKT5G5yh/polysemantic-attention-head-in-a-4-layer-transformer>. LessWrong Blog.

Kantamneni, S.; Engels, J.; Rajamanoharan, S.; Tegmark, M.; and Nanda, N. 2025. Are Sparse Autoencoders Useful? A Case Study in Sparse Probing. In *Forty-second International Conference on Machine Learning*.

Kissane, C.; Krzyzanowski, R.; Bloom, J. I.; Conmy, A.; and Nanda, N. 2024. Interpreting attention layer outputs with sparse autoencoders. *arXiv preprint arXiv:2406.17759*.

Lecomte, V.; Thaman, K.; Schaeffer, R.; Bashkansky, N.; Chow, T.; and Koyejo, S. 2024. What Causes Polysemanticity? An Alternative Origin Story of Mixed Selectivity from Incidental Causes. In *ICLR 2024 Workshop on Representational Alignment*.

Li, A. J.; Srinivas, S.; Bhalla, U.; and Lakkaraju, H. 2025. Interpretability Illusions with Sparse Autoencoders: Evaluating Robustness of Concept Representations. *arXiv preprint arXiv:2505.16004*.

Lieberum, T.; Rajamanoharan, S.; Conmy, A.; Smith, L.; Sonnerat, N.; Varma, V.; Kramar, J.; Dragan, A.; Shah, R.; and Nanda, N. 2024. Gemma Scope: Open Sparse Autoencoders Everywhere All At Once on Gemma 2. In Belinkov, Y.; Kim, N.; Jumelet, J.; Mohebbi, H.; Mueller, A.; and Chen, H., eds., *Proceedings of the 7th BlackboxNLP*

Workshop: Analyzing and Interpreting Neural Networks for NLP, 278–300. Miami, Florida, US: Association for Computational Linguistics.

Lin, J. 1991. Divergence measures based on the Shannon entropy. *IEEE Transactions on Information Theory*, 37(1): 145–151.

Luo, X.; Rechardt, A.; Sun, G.; Nejad, K. K.; Yáñez, F.; Yilmaz, B.; Lee, K.; Cohen, A. O.; Borghesani, V.; Pashkov, A.; et al. 2025. Large language models surpass human experts in predicting neuroscience results. *Nature human behaviour*, 9(2): 305–315.

Maas, A. L.; Daly, R. E.; Pham, P. T.; Huang, D.; Ng, A. Y.; and Potts, C. 2011. Learning Word Vectors for Sentiment Analysis. In *Proceedings of the 49th Annual Meeting of the Association for Computational Linguistics: Human Language Technologies*, 142–150. Portland, Oregon, USA: Association for Computational Linguistics.

Marshall, S. C.; and Kirchner, J. H. 2024. Understanding polysemanticity in neural networks through coding theory. *arXiv preprint arXiv:2401.17975*.

Meng, K.; Bau, D.; Andonian, A. J.; and Belinkov, Y. 2022. Locating and Editing Factual Associations in GPT. In Oh, A. H.; Agarwal, A.; Belgrave, D.; and Cho, K., eds., *Advances in Neural Information Processing Systems*.

Meng, K.; Sharma, A. S.; Andonian, A. J.; Belinkov, Y.; and Bau, D. 2023. Mass-Editing Memory in a Transformer. In *The Eleventh International Conference on Learning Representations*.

Minegishi, G.; Furuta, H.; Iwasawa, Y.; and Matsuo, Y. 2025. Rethinking Evaluation of Sparse Autoencoders through the Representation of Polysemous Words. In *The Thirteenth International Conference on Learning Representations*.

Morcos, A. S.; Barrett, D. G.; Rabinowitz, N. C.; and Botvinick, M. 2018. On the importance of single directions for generalization. In *International Conference on Learning Representations*.

Nguyen, A.; Yosinski, J.; and Clune, J. 2016. Multifaceted feature visualization: Uncovering the different types of features learned by each neuron in deep neural networks. *arXiv preprint arXiv:1602.03616*.

Olah, C.; Mordvintsev, A.; and Schubert, L. 2017. Feature Visualization. *Distill*. [Https://distill.pub/2017/feature-visualization](https://distill.pub/2017/feature-visualization).

Pach, M.; Karthik, S.; Bouniot, Q.; Belongie, S.; and Akata, Z. 2025. Sparse autoencoders learn monosemantic features in vision-language models. *arXiv preprint arXiv:2504.02821*.

Rajamanoharan, S.; Conmy, A.; Smith, L.; Lieberum, T.; Varma, V.; Kramár, J.; Shah, R.; and Nanda, N. 2024a. Improving dictionary learning with gated sparse autoencoders. *arXiv preprint arXiv:2404.16014*.

Rajamanoharan, S.; Lieberum, T.; Sonnerat, N.; Conmy, A.; Varma, V.; Kramár, J.; and Nanda, N. 2024b. Jumping ahead: Improving reconstruction fidelity with jumprelu sparse autoencoders. *arXiv preprint arXiv:2407.14435*.

Rivière, M.; Pathak, S.; Sessa, P. G.; Hardin, C.; Bhupatiraju, S.; Hussenot, L.; Mesnard, T.; Shahriari, B.; Ramé, A.; Ferret, J.; Liu, P.; Tafti, P.; Friesen, A.; Casbon, M.; Ramos, S.; Kumar, R.; Lan, C. L.; Jerome, S.; Tsitsulin, A.; Vieillard, N.; Stanczyk, P.; Girgin, S.; Momchev, N.; Hoffman, M.; Thakoor, S.; Grill, J.-B.; Neyshabur, B.; Bachem, O.; Walton, A.; Severyn, A.; Parrish, A.; Ahmad, A.; Hutchinson, A.; Abdagic, A.; Carl, A.; Shen, A.; Brock, A.; Coenen, A.; Laforge, A.; Paterson, A.; Bastian, B.; Piot, B.; Wu, B.; Royal, B.; Chen, C.; Kumar, C.; Perry, C.; Welty, C.; Choquette-Choo, C. A.; Sinopalnikov, D.; Weinberger, D.; Vijaykumar, D.; Rogozinska, D.; Herbison, D.; Bandy, E.; Wang, E.; Noland, E.; Moreira, E.; Senter, E.; Eltyshev, E.; Visin, F.; Rasskin, G.; Wei, G.; Cameron, G.; Martins, G.; Hashemi, H.; Klimczak-Plucinska, H.; Batra, H.; Dhand, H.; Nardini, I.; Mein, J.; Zhou, J.; Svensson, J.; Stanway, J.; Chan, J.; Zhou, J. P.; Carrasqueira, J.; Iljazi, J.; Becker, J.; Fernandez, J.; van Amersfoort, J.; Gordon, J.; Lipschultz, J.; Newlan, J.; yeong Ji, J.; Mohamed, K.; Badola, K.; Black, K.; Millican, K.; McDonell, K.; Nguyen, K.; Sodhia, K.; Greene, K.; Sjöstrand, L. L.; Usui, L.; Sifre, L.; Heuermann, L.; Lago, L.; and McNealus, L. 2024. Gemma 2: Improving Open Language Models at a Practical Size. *CoRR*, abs/2408.00118.

Rodriguez, P.; Blaas, A.; Klein, M.; Zappella, L.; Apostoloff, N.; marco cuturi; and Suau, X. 2025. Controlling Language and Diffusion Models by Transporting Activations. In *The Thirteenth International Conference on Learning Representations*.

Saravia, E.; Liu, H.-C. T.; Huang, Y.-H.; Wu, J.; and Chen, Y.-S. 2018. CARER: Contextualized Affect Representations for Emotion Recognition. In *Proceedings of the 2018 Conference on Empirical Methods in Natural Language Processing*, 3687–3697. Brussels, Belgium: Association for Computational Linguistics.

Scherlis, A.; Sachan, K.; Jermyn, A. S.; Benton, J.; and Shlegeris, B. 2022. Polysemanticity and capacity in neural networks. *arXiv preprint arXiv:2210.01892*.

Sharkey, L.; Chughtai, B.; Batson, J.; Lindsey, J.; Wu, J.; Bushnaq, L.; Goldowsky-Dill, N.; Heimersheim, S.; Ortega, A.; Bloom, J.; et al. 2025. Open problems in mechanistic interpretability. *arXiv preprint arXiv:2501.16496*.

Shu, D.; Wu, X.; Zhao, H.; Rai, D.; Yao, Z.; Liu, N.; and Du, M. 2025. A Survey on Sparse Autoencoders: Interpreting the Internal Mechanisms of Large Language Models. *CoRR*, abs/2503.05613.

Socher, R.; Perelygin, A.; Wu, J.; Chuang, J.; Manning, C. D.; Ng, A.; and Potts, C. 2013. Recursive Deep Models for Semantic Compositionality Over a Sentiment Treebank. In *Proceedings of the 2013 Conference on Empirical Methods in Natural Language Processing*, 1631–1642. Seattle, Washington, USA: Association for Computational Linguistics.

Suau, X.; Delobelle, P.; Metcalf, K.; Joulin, A.; Apostoloff, N.; Zappella, L.; and Rodríguez, P. 2024. Whispering experts: neural interventions for toxicity mitigation in language models. In *Proceedings of the 41st International Conference on Machine Learning*, ICML’24. JMLR.org.

Sun, J.; Baskaran, S.; Wu, Z.; Sklar, M.; Potts, C.; and Geiger, A. 2025a. HyperSteer: Activation Steering at Scale with Hypernetworks. *arXiv preprint arXiv:2506.03292*.

Sun, X.; Stolfo, A.; Engels, J.; Wu, B.; Rajamanoharan, S.; Sachan, M.; and Tegmark, M. 2025b. Dense SAE Latents Are Features, Not Bugs. *arXiv preprint arXiv:2506.15679*.

Touvron, H.; Martin, L.; Stone, K.; Albert, P.; Almahairi, A.; Babaei, Y.; Bashlykov, N.; Batra, S.; Bhargava, P.; Bhosale, S.; et al. 2023. Llama 2: Open foundation and fine-tuned chat models. *arXiv preprint arXiv:2307.09288*.

Vig, J.; Gehrmann, S.; Belinkov, Y.; Qian, S.; Nevo, D.; Singer, Y.; and Shieber, S. 2020. Investigating Gender Bias in Language Models Using Causal Mediation Analysis. In Larochelle, H.; Ranzato, M.; Hadsell, R.; Balcan, M.; and Lin, H., eds., *Advances in Neural Information Processing Systems*, volume 33, 12388–12401. Curran Associates, Inc.

Zhang, X.; Zhao, J.; and LeCun, Y. 2015. Character-level Convolutional Networks for Text Classification. In Cortes, C.; Lawrence, N.; Lee, D.; Sugiyama, M.; and Garnett, R., eds., *Advances in Neural Information Processing Systems*, volume 28. Curran Associates, Inc.

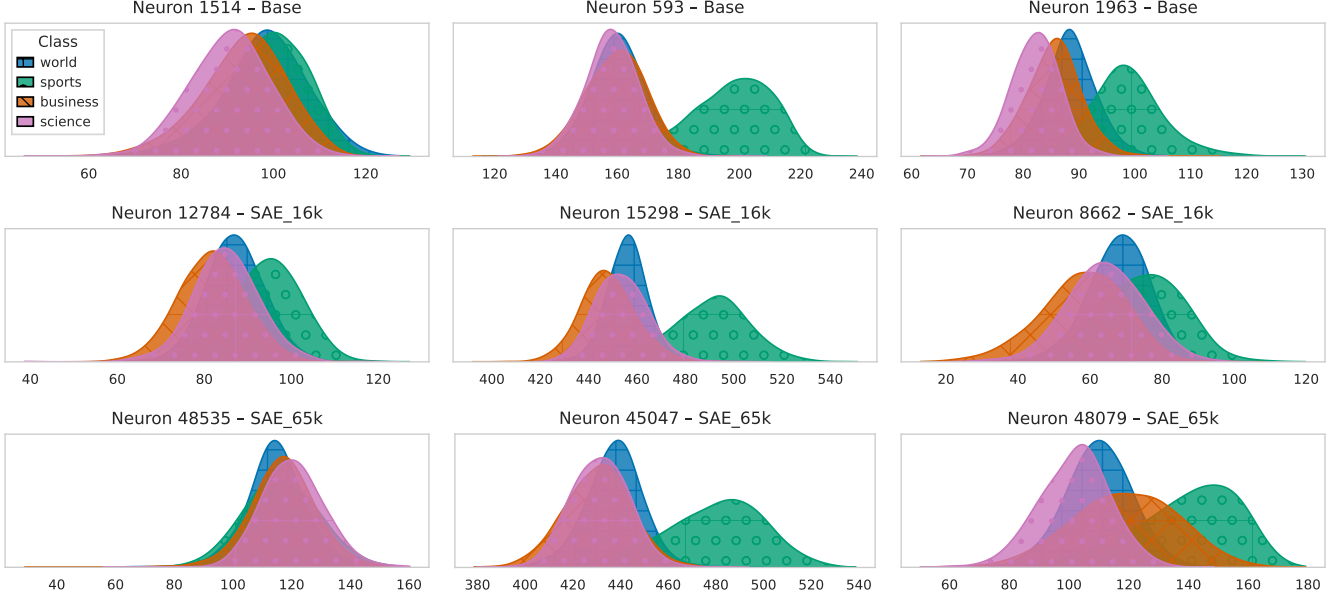


Figure 4: Across base model and SAEs (SAE-16k, SAE-65k), neurons exhibit varying degrees of separability in their activations on AG News dataset.

Table 3: Concept Erasure Detailed metrics  $D_{\text{Acc}}$ ,  $D'_{\text{Acc}}$ ,  $D_{\text{Conf}}$ , and  $D'_{\text{Conf}}$

| Type                      | Method   | IMDB                      |                              |                            |                               | AG News                   |                              |                            |                               | Emotions                  |                              |                            |                               | DBpedia                   |                              |                            |                               | SST2                      |                              |                            |                               |
|---------------------------|----------|---------------------------|------------------------------|----------------------------|-------------------------------|---------------------------|------------------------------|----------------------------|-------------------------------|---------------------------|------------------------------|----------------------------|-------------------------------|---------------------------|------------------------------|----------------------------|-------------------------------|---------------------------|------------------------------|----------------------------|-------------------------------|
|                           |          | $D_{\text{Acc}} \uparrow$ | $D'_{\text{Acc}} \downarrow$ | $D_{\text{Conf}} \uparrow$ | $D'_{\text{Conf}} \downarrow$ | $D_{\text{Acc}} \uparrow$ | $D'_{\text{Acc}} \downarrow$ | $D_{\text{Conf}} \uparrow$ | $D'_{\text{Conf}} \downarrow$ | $D_{\text{Acc}} \uparrow$ | $D'_{\text{Acc}} \downarrow$ | $D_{\text{Conf}} \uparrow$ | $D'_{\text{Conf}} \downarrow$ | $D_{\text{Acc}} \uparrow$ | $D'_{\text{Acc}} \downarrow$ | $D_{\text{Conf}} \uparrow$ | $D'_{\text{Conf}} \downarrow$ | $D_{\text{Acc}} \uparrow$ | $D'_{\text{Acc}} \downarrow$ | $D_{\text{Conf}} \uparrow$ | $D'_{\text{Conf}} \downarrow$ |
| Base                      | APP      | 0.390                     | 0.013                        | 0.135                      | -0.058                        | 0.342                     | 0.007                        | 0.243                      | -0.013                        | 0.060                     | 0.015                        | 0.085                      | -0.003                        | 0.126                     | 0.012                        | 0.100                      | -0.003                        | 0.283                     | 0.009                        | 0.078                      | -0.042                        |
|                           | Aura     | 0.036                     | 0.075                        | 0.039                      | 0.063                         | 0.104                     | 0.033                        | 0.161                      | 0.071                         | 0.020                     | 0.042                        | 0.019                      | 0.019                         | 0.169                     | 0.077                        | 0.094                      | 0.030                         | 0.022                     | 0.143                        | -0.017                     | 0.017                         |
|                           | Range    | 0.799                     | 0.733                        | 0.323                      | 0.290                         | 0.253                     | 0.189                        | 0.314                      | 0.226                         | 0.119                     | 0.090                        | 0.201                      | 0.101                         | 0.357                     | 0.188                        | 0.194                      | 0.085                         | 0.434                     | 0.355                        | 0.281                      | 0.251                         |
|                           | Adaptive | 0.455                     | 0.348                        | 0.244                      | 0.196                         | 0.139                     | 0.092                        | 0.209                      | 0.126                         | 0.093                     | 0.064                        | 0.138                      | 0.056                         | 0.238                     | 0.117                        | 0.135                      | 0.036                         | 0.157                     | 0.127                        | 0.174                      | 0.150                         |
|                           | Full     | 0.828                     | 0.805                        | 0.333                      | 0.321                         | 0.251                     | 0.181                        | 0.313                      | 0.242                         | 0.119                     | 0.086                        | 0.203                      | 0.095                         | 0.363                     | 0.193                        | 0.196                      | 0.093                         | 0.458                     | 0.334                        | 0.309                      | 0.278                         |
| SAE width: 65k<br>l0: 93  | APP      | 0.698                     | 0.102                        | 0.378                      | 0.081                         | 0.626                     | 0.022                        | 0.411                      | -0.030                        | 0.275                     | 0.037                        | 0.275                      | 0.0001                        | 0.411                     | 0.011                        | 0.215                      | -0.003                        | 0.768                     | 0.125                        | 0.404                      | 0.166                         |
|                           | Aura     | 0.324                     | 0.001                        | 0.199                      | -0.009                        | 0.602                     | 0.013                        | 0.410                      | 0.044                         | 0.370                     | 0.039                        | 0.307                      | 0.007                         | 0.413                     | 0.055                        | 0.216                      | 0.002                         | 0.650                     | 0                            | 0.124                      | -0.052                        |
|                           | Range    | 0.745                     | 0.694                        | 0.406                      | 0.387                         | 0.672                     | 0.083                        | 0.434                      | 0.313                         | 0.417                     | 0.274                        | 0.379                      | 0.356                         | 0.411                     | 0.158                        | 0.218                      | 0.162                         | 0.830                     | 0.803                        | 0.487                      | 0.479                         |
|                           | Adaptive | 0.735                     | 0.600                        | 0.398                      | 0.332                         | 0.671                     | 0.077                        | 0.433                      | 0.223                         | 0.415                     | 0.235                        | 0.377                      | 0.296                         | 0.410                     | 0.188                        | 0.217                      | 0.134                         | 0.791                     | 0.716                        | 0.468                      | 0.438                         |
|                           | Full     | 0.757                     | 0.755                        | 0.407                      | 0.407                         | 0.673                     | 0.067                        | 0.434                      | 0.427                         | 0.418                     | 0.299                        | 0.380                      | 0.378                         | 0.413                     | 0.138                        | 0.219                      | 0.200                         | 0.833                     | 0.833                        | 0.490                      | 0.490                         |
| SAE width: 16k<br>l0: 116 | APP      | 0.660                     | 0.176                        | 0.350                      | 0.108                         | 0.621                     | 0.036                        | 0.343                      | -0.025                        | 0.293                     | 0.025                        | 0.270                      | 0.0007                        | 0.331                     | 0.019                        | 0.149                      | -0.003                        | 0.539                     | 0.093                        | 0.430                      | 0.195                         |
|                           | Aura     | 0.578                     | 0.029                        | 0.259                      | 0.011                         | 0.622                     | 0.024                        | 0.342                      | 0.057                         | 0.360                     | 0.035                        | 0.297                      | 0.016                         | 0.333                     | 0.075                        | 0.151                      | 0.011                         | 0.083                     | 0                            | 0.147                      | -0.021                        |
|                           | Range    | 0.734                     | 0.634                        | 0.378                      | 0.373                         | 0.404                     | 0.047                        | 0.345                      | 0.227                         | 0.399                     | 0.302                        | 0.341                      | 0.332                         | 0.334                     | 0.126                        | 0.152                      | 0.099                         | 0.552                     | 0.277                        | 0.4553                     | 0.4455                        |
|                           | Adaptive | 0.732                     | 0.607                        | 0.376                      | 0.356                         | 0.430                     | 0.069                        | 0.334                      | 0.162                         | 0.399                     | 0.275                        | 0.341                      | 0.296                         | 0.334                     | 0.156                        | 0.152                      | 0.081                         | 0.550                     | 0.277                        | 0.449                      | 0.420                         |
|                           | Full     | 0.746                     | 0.744                        | 0.378                      | 0.378                         | 0.404                     | 0.082                        | 0.346                      | 0.340                         | 0.399                     | 0.354                        | 0.3418                     | 0.3413                        | 0.335                     | 0.148                        | 0.153                      | 0.152                         | 0.578                     | 0.578                        | 0.455                      | 0.455                         |
| SAE width: 65k<br>l0: 197 | APP      | 0.721                     | 0.102                        | 0.320                      | 0.015                         | 0.640                     | 0.028                        | 0.417                      | -0.029                        | 0.273                     | 0.025                        | 0.274                      | -0.009                        | 0.390                     | 0.028                        | 0.229                      | -0.005                        | 0.882                     | 0.144                        | 0.380                      | 0.084                         |
|                           | Aura     | 0.397                     | 0                            | 0.133                      | -0.064                        | 0.646                     | 0.034                        | 0.416                      | 0.024                         | 0.340                     | 0.035                        | 0.314                      | -0.003                        | 0.392                     | 0.095                        | 0.233                      | -0.001                        | 0.767                     | 0                            | 0.136                      | -0.097                        |
|                           | Range    | 0.807                     | 0.781                        | 0.404                      | 0.392                         | 0.655                     | 0.360                        | 0.434                      | 0.388                         | 0.403                     | 0.274                        | 0.388                      | 0.366                         | 0.391                     | 0.098                        | 0.235                      | 0.129                         | 0.901                     | 0.896                        | 0.454                      | 0.453                         |
|                           | Adaptive | 0.796                     | 0.682                        | 0.390                      | 0.321                         | 0.655                     | 0.360                        | 0.434                      | 0.326                         | 0.401                     | 0.231                        | 0.384                      | 0.280                         | 0.391                     | 0.133                        | 0.235                      | 0.088                         | 0.896                     | 0.876                        | 0.444                      | 0.429                         |
|                           | Full     | 0.821                     | 0.813                        | 0.405                      | 0.404                         | 0.655                     | 0.387                        | 0.434                      | 0.433                         | 0.403                     | 0.317                        | 0.388                      | 0.386                         | 0.392                     | 0.175                        | 0.236                      | 0.216                         | 0.913                     | 0.913                        | 0.4566                     | 0.4565                        |
| SAE width: 16k<br>l0: 285 | APP      | 0.828                     | 0.513                        | 0.257                      | 0.135                         | 0.670                     | 0.041                        | 0.353                      | -0.002                        | 0.254                     | 0.043                        | 0.236                      | 0.014                         | 0.321                     | 0.047                        | 0.148                      | 0.001                         | 0.894                     | 0.851                        | 0.268                      | 0.222                         |
|                           | Aura     | 0.574                     | 0.003                        | 0.199                      | 0.039                         | 0.674                     | 0.123                        | 0.348                      | 0.008                         | 0.301                     | 0.032                        | 0.270                      | 0.022                         | 0.323                     | 0.164                        | 0.152                      | 0.040                         | 0.857                     | 0.030                        | 0.190                      | 0.010                         |
|                           | Range    | 0.829                     | 0.812                        | 0.260                      | 0.256                         | 0.673                     | 0.226                        | 0.360                      | 0.295                         | 0.370                     | 0.261                        | 0.345                      | 0.334                         | 0.322                     | 0.140                        | 0.153                      | 0.095                         | 0.890                     | 0.842                        | 0.272                      | 0.271                         |
|                           | Adaptive | 0.829                     | 0.802                        | 0.258                      | 0.237                         | 0.674                     | 0.245                        | 0.360                      | 0.217                         | 0.370                     | 0.252                        | 0.3441                     | 0.276                         | 0.322                     | 0.176                        | 0.152                      | 0.068                         | 0.892                     | 0.868                        | 0.268                      | 0.264                         |
|                           | Full     | 0.8293                    | 0.8292                       | 0.26088                    | 0.2607                        | 0.675                     | 0.534                        | 0.3607                     | 0.3603                        | 0.370                     | 0.313                        | 0.345                      | 0.344                         | 0.323                     | 0.169                        | 0.129                      | 0.085                         | 0.886                     | 0.27241                      | 0.27240                    |                               |

## A AG News Neurons Activation

As shown in Figure 4, certain neurons in both the base model and SAEs (e.g., leftmost plots) exhibit considerable overlap in their activation distributions across the four classes, indicating limited class discrimination. In contrast, neurons shown in the middle and right columns reveal more separable activation patterns.

## B The Histogram implementation of KDE

Directly computing the probability densities  $f_{h_j^l|c_i}(x)$  at inference time is computationally expensive, as it requires comparing each query activation  $x$  against all  $N$  training activations for every neuron-concept pair. To mitigate this

overhead, we adopt a histogram-based kernel density estimation (KDE) approach.

During training, we discretize each activation distribution into  $B$  uniform-width histogram bins and store the corresponding bin centers, counts, bandwidths, and normalization constants. At inference time, we compute densities by evaluating each query activation only against these  $B$  stored bin centers, avoiding costly comparisons with the full training set. This enables efficient computation using precomputed log-counts and normalization factors, greatly accelerating the density estimation process.

In all experiments, we fix  $B = 2048$ . Let  $F$  denote the number of neurons (i.e., distributions),  $N$  the number of training samples, and  $Q$  the number of query points. Then

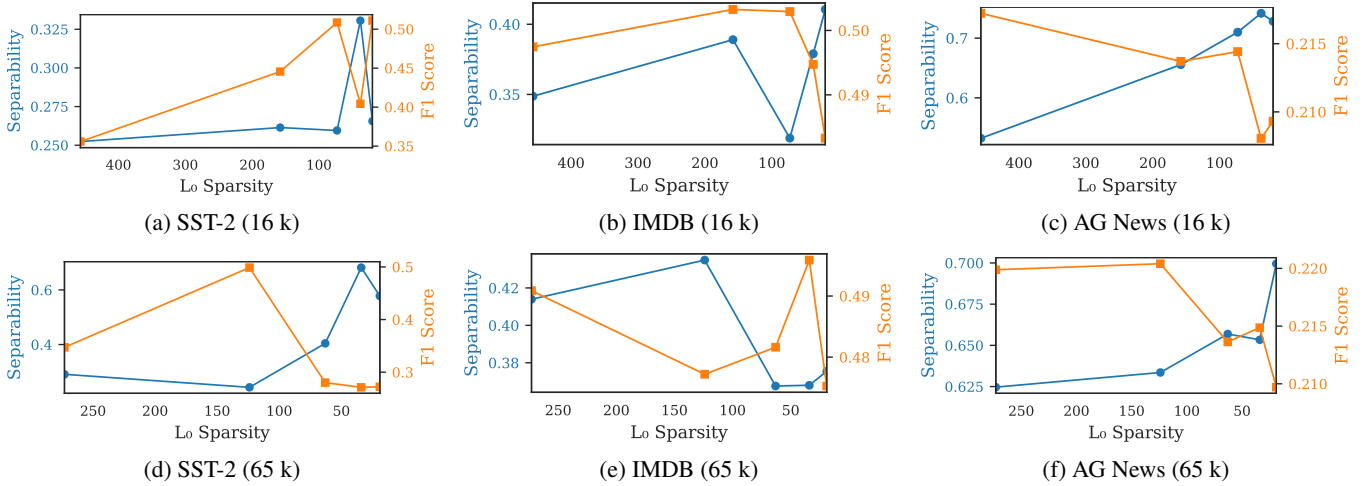


Figure 5: While increased sparsity generally enhances concept separability, excessive sparsity can sometimes lead to a significant drop in separability.

the computational and memory complexity of our method compared to naïve KDE is:

- **Inference time:**

Histogram-KDE:  $\mathcal{O}(FBQ)$ ,    Naïve KDE:  $\mathcal{O}(FNQ)$

- **Memory footprint:**

Histogram-KDE:  $\mathcal{O}(FB)$ ,    Naïve KDE:  $\mathcal{O}(FN)$

Since  $B \ll N$ , this substitution yields an approximate  $\frac{N}{B}$ -fold improvement in both inference speed and memory usage. While the approximation may introduce a negligible loss in density accuracy, it provides substantial practical gains in scalability.

## C Details of Experiments

The detailed metrics ( $D_{\text{Acc}}$ ,  $D'_{\text{Acc}}$ ,  $D_{\text{Conf}}$ , and  $D'_{\text{Conf}}$ ) before subtraction are reported in Table 3; the corresponding values after subtraction are presented in the main paper (Table 2).

## D Separability Score Trend in Layer 24

As shown in Figure 5, there is a general trend that increasing sparsity tends to improve separability. However, this is not always the case. For example, in subplots (a), (b), and (e), increased sparsity actually leads to reduced separability. Similarly, while performance typically decreases with higher sparsity, there are notable exceptions. In subplots (a) and (e) for instance, performance improves despite the activations becoming more sparse.

## E All SAE Neurons Analysis

While our salient neuron analysis provides valuable insight into the most strongly responding neurons, it considers only a narrow slice of the activation space (specifically, the top 50 neurons per concept). This limited scope may miss neurons that, although not highly ranked by mean activation, are still consistently active across multiple concepts and contribute

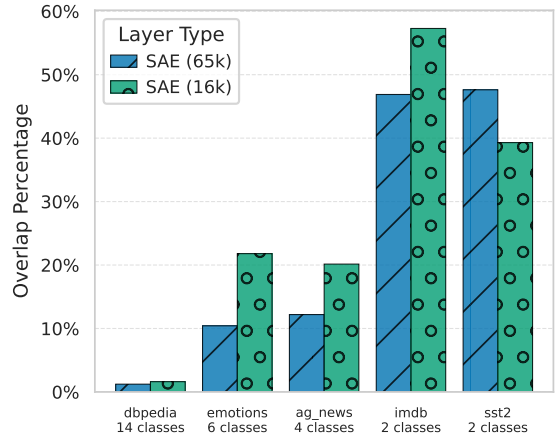


Figure 6: 65k SAEs show lower overlap than 16k, further supporting that greater capacity enables more distinct neuron-to-concept mappings.

to polysemy. To address this limitation, we broaden our analysis to include all neurons that exhibit non-zero activation for any concept, offering a more comprehensive view of concept overlap beyond the most salient neurons. This extended analysis is conducted only for SAEs, since in the dense base model, all neurons are active across all inputs, rendering such overlap statistics uninformative. The results are shown in Figure 6, which reports the intersection-over-union of active neurons across concepts. By capturing both highly active and more subtly engaged neurons, this analysis reveals a complete picture of polysemantic behavior. Consistent with our earlier findings shown in Figure 1, we observe that higher-capacity SAEs (e.g., 65k dimensions) exhibit lower neuron overlap than their lower-capacity counterparts across all datasets except SST2. Together, Figures 1 and 6 demonstrate that while SAEs significantly reduce polysemy, they do not eliminate it entirely. Polysemantc neurons remain present, albeit to a lesser extent.